The Pressures of Partial Crystallization along the Galápagos Spreading Center

Research Thesis

Submitted in partial fulfillment of the requirements for graduation

with research distinction in Earth Sciences in the undergraduate colleges

of The Ohio State University

By

Katherine A. Haines

The Ohio State University

2016

Approved by

Dr. Michael Barton, Advisor

School of Earth Sciences

TABLE OF CONTENTS

ABSTRACT

As part of a larger project aimed at understanding the magma plumbing systems and magmatic processes responsible for crust formation at divergent plate margins, we have begun a study of the Galápagos Spreading Center (GSC), an intermediate spreading ridge off the west coast of South America and connected to the East Pacific Rise. This ridge is of interest because it passes close to the Galápagos Islands, allowing the effects of a mantle plume on sub-ridge processes and magma plumbing systems to be examined. In addition, the effects of ridge-ridge intersection, ridge propagation, and ridge offsets by transform faults on magma evolution can be examined. Published compositional data for glasses collected along the ridge were used to calculate pressures of partial crystallization and to examine variations in magma chemistry along the ridge. To aid interpretation of the results, the ridge was divided into 12 segments based on sample distribution and the occurrence of ridge offsets. Calculated pressures for most segments range between 100 and 300 MPa, and indicate depths of partial crystallization of ~3–9 km. This suggests that partial crystallization and hence crustal accretion occurs mostly near the base of the crust. The range of pressures for some segments is relatively large with maximum calculated values of 500–750 MPa. Near the major transform fault at ~85^{O}W, the calculated maximum pressure is 741 MPa and the average pressure is ~300 MPa. It is unlikely that the calculated high pressures represent the true pressure of partial crystallization. The compositions of some magmas may result from processes other than simple crystallization. Correlations between pressure and MgO, between Na_2O and MgO, P_2O_5 and K_2O, and between Na_8 and longitude suggest that the processes operating beneath this ridge are complex. Near the transform fault MgO vs pressure shows a negative correlation with an R^2 value of 0.546. Such trends are inconsistent with magma evolution via crystallization alone suggesting that crystallization was accompanied by interaction with pre-existing crust. Modification of magma compositions through assimilation of oceanic crust probably accounts for the wide range of pressures calculated for samples from some ridge segments.

ACKNOWLEDGEMENTS

I would like to thank Christina Zerda, Jameson Scott, Dr. Anne Carey and my research advisor Dr. Michael Barton for their help and support during my research experience. Support was also provided by the Shell Exploration and Production Company, the Friends of Orton Hall funding opportunity and from the William J. Bushman Scholarship received in 2015. These scholarships and opportunities allowed me to focus on my research during this past academic year. I would also like to mention the other undergraduates in my research group: Yoko Miyakawa and Lienne Sethna. Both gave valuable support and input during our senior year at Ohio State University. A special thanks to my husband for understanding and supporting me through this process, I could not have done it without him.

LIST OF FIGURES

LIST OF TABLES

INTRODUCTION

The generation of new oceanic crust and lithosphere occurs at mid-ocean ridges (MOR), so that studies of ridges are essential to understand mantle processes. The MOR systems form the longest mountain ranges on the Earth, and mark the sites where plates continually spread apart to create new crust. Spreading rates differ along different ridge systems, hence the rate of crust formation is variable. The morphology of ridge systems depends on spreading rate and therefore to the amount of heat lost at the ridge axis.

The mantle cannot be sampled directly, and models of oceanic crustal accretion must be based on analysis of samples of lava erupted along ridge systems. Currently, there are three accepted models of crustal accretion (Figure 1). The earliest model for accretion of oceanic crust was published in the 1970's and was largely based on observations from ophiolites (Bryan and Moore, 1977; Dewey and Kidd, 1977). In this model, known as the gabbro glacier model (Figure 1a), magma crystallizes in a single melt lens, or magma chamber, and the precipitated crystals accumulate along the floor and walls, forming a solid that flows laterally and downwards away from the melt lens as the crust spreads from the ridge axis in a manner similar to that of the solid-state flow of a glacier (Sleep, 1975; Dewey and Kidd, 1977; Quick and Denlinger, 1993). Early workers thought that the melt body extended over a depth range of several kilometers, but interpretation of seismic data in the 1980's indicated that the melt body is a sill-like lens of melt that is located at relatively shallow depths and is typically only a few 10s of meters thick (Sinton and Detrick, 1992; Rubin *et al.*, 2009). A significant consequence of this model is that crystallization occurs in a single magma body and therefore over a narrow range of depth.

The second model is the crystal "mush" model devised in the early 1990's. With this model, a thin, shallow, magma lens is underlain by a crystal "mush" extending down to the base of the crust (Figure 1b). The magma lens feeds surface eruptions, whereas crystallization in the "mush" zone forms the gabbro layer of the crust via in-situ crystallization (Boudier *et al.*, 1996; Sinton and Detrick, 1992). An obvious consequence of this model is that crystallization, and hence crustal accretion, occurs over a range of depths in the crust.

The third model is referred to as the many sill or sheeted sill model (Figure 1c). This model consists of multiple sill-like magma lenses located at various depths throughout the crust beneath the ridge axis. The presence of sills at multiple depths allows crystallization and hence crustal accretion over a range of depths in the crust (Kelemen *et al.*, 1997; Bédard *et al.*, 1988; Kelemen and Aharonov, 1998).

In principle, models for crustal accretion can be tested by using petrological methods to determine the depths of partial crystallization of magmas erupted along the GSC. This is the main objective of the research described in this thesis. However, the compositions of magmas erupted along the GSC are also examined to provide the foundation for future studies that examine the intracrustal evolutionary history of these magmas and that provide constraints on models of oceanic crustal composition.

(a)

(b)

(c)

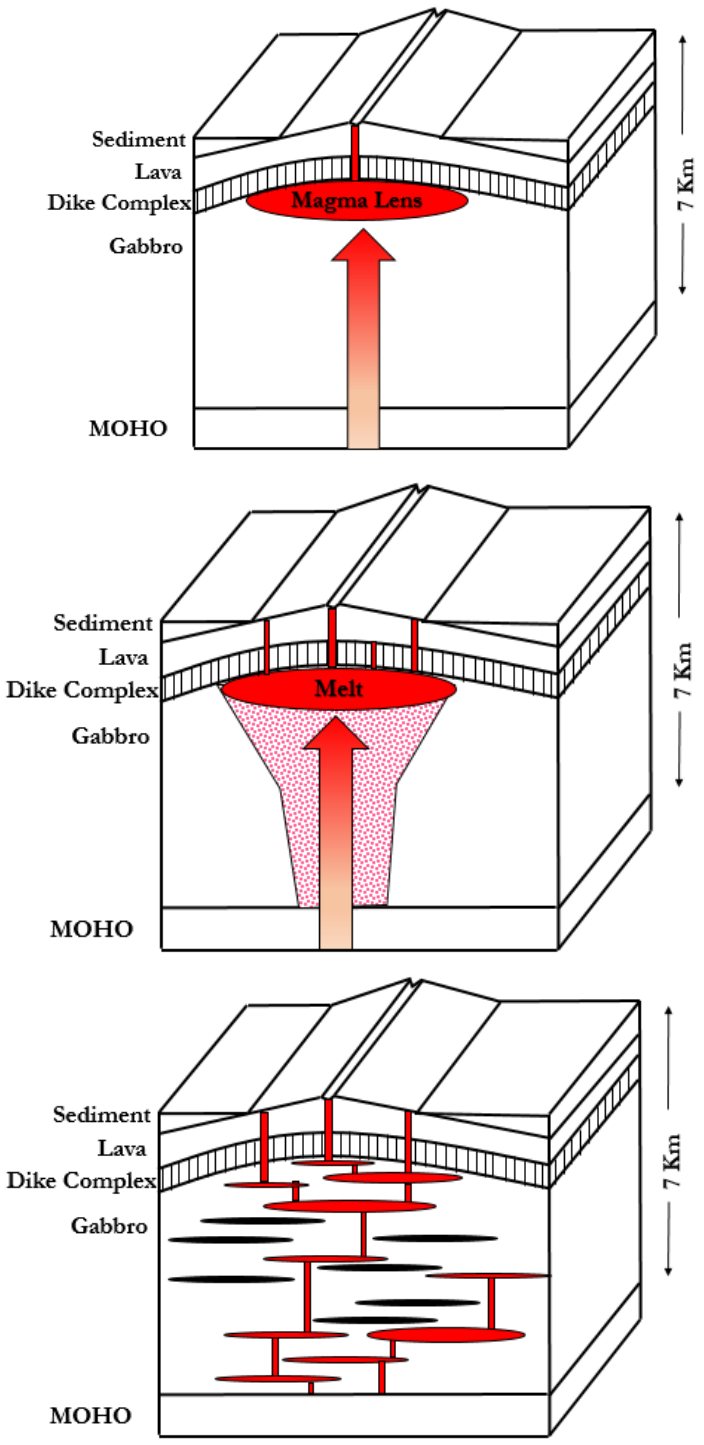

Figure 1: Three models of crustal accretion. (a) The Gabbro-glacial model. (b) The crystal mush model. This shows that a "mush" that extends down to the mantle boundary can exist and allows for crystallization at a range of depths. (c) The many sill model. Melt from the mantle flows from one sill to the next, also allowing for a range of crystallization.

GEOLOGIC SETTING

The Galápagos Spreading Center (GSC) is an intermediate spreading ridge north of the Galápagos Archipelago. The spreading center lies between the East Pacific Rise (EPR) and the west coast of South America (Figure 2). The GSC separates the Cocos from the Nazca Plates as both of these from the Pacific plate on the western edge of the spreading center at a triple junction. The GSC is therefore also known as the Cocos-Nazca Spreading Center (Hey, 1977).

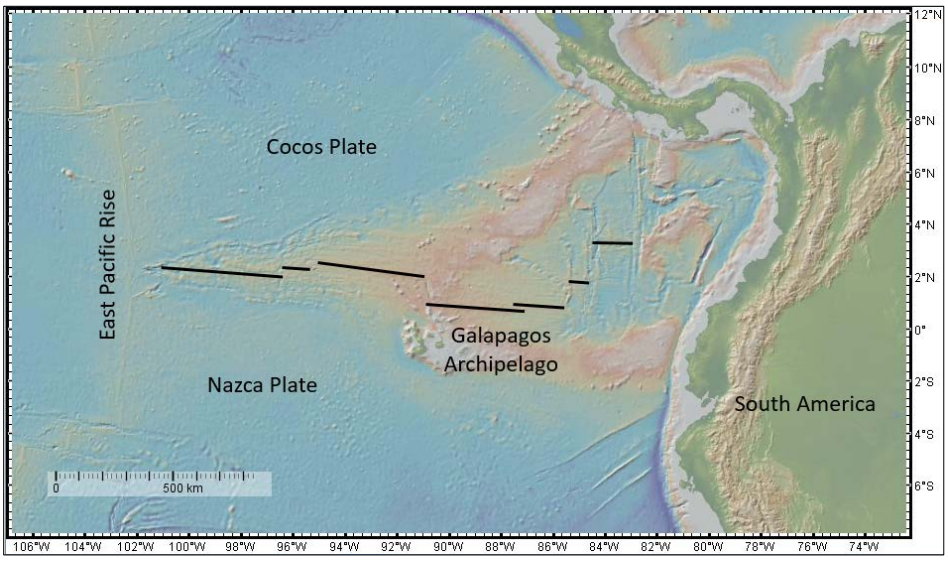

Figure 2: Regional map of the GSC and the Galápagos Islands. The Nazca, East Pacific and the Cocos Plates all meet at a triple junction on the western edge of the GSC. Map was generated using *GeoMapApp*.

The full spreading rate ranges from 40-65 mm/year with an average of 54 mm/year (Gale *et al.*, 2014). Six major transform faults occur along the ridge as well as an overlapping spreading center at 87°W. The Galápagos plume is thought lie beneath the western parts of the islands Fernandina and Isabela (Harpp and Geist, 2002) and lies to the south of the ridge. Plume-ridge interaction makes the GSC unique and makes this ridge ideal for studying the relationship between plate spreading and the processes that occur in the Earth's mantle. Because the plume is located some distance to the south of the Galápagos Spreading Center, the Galápagos Spreading Center will primarily provide information about mid ocean ridge processes (Harpp and Geist, 2002).

Various morphological features indicate effects of the hotspot and magma supply in the area. Besides the Galápagos Archipelago, these features include the Cocos ridge, the Carnegie ridge, the Galápagos platform and the Wolf-Darwin lineament (Canales *et al.*, 2002). The Wolf-Darwin lineament is a "bathymetric high that connects the Galápagos platform to the GSC (Harpp and Geist, 2002).

Seismic data can help determine relative temperatures beneath ridge systems. Slow velocity data indicate warmer temperatures whereas higher velocity indicates cooler temperatures (Canales *et al.*, 2002). Using *GeoMapApp*, a profile created along the GSC shows the change of topography for the GSC (Figure 3). The Galápagos Archipelago starts around a longitude of 92°W and ends around

89°W, and if the hotspot is near or beneath the islands, uplift would occur in this range. Figure 3 displays the highest elevation is in that range of longitudes.

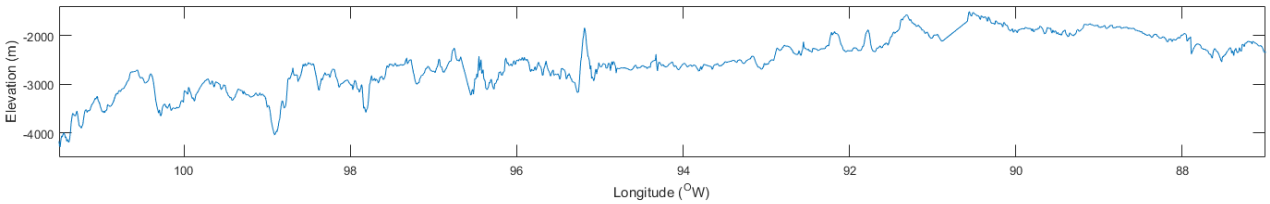

Figure 3: Elevation change from West to East. Note that around the Galápagos islands, the depth decreases, likely due to the swell caused by the Galápagos hotspot.

The axial ridge profile also changes from West to East along the GSC. Using the *GeoMapApp*, three profiles were created to show the elevation versus latitude (Figure 4). Figure 4a displays the profile for the axial ridge at an average longitude of 97.2°W. Figure 4b displays the profile view of the axial ridge at an average longitude of 89.6°W and Figure 4c displays the profile view of the axial ridge with an average longitude of 86.3°W. All three profiles are different, with the highest elevation in 4b, closest to the Galápagos Archipelago.

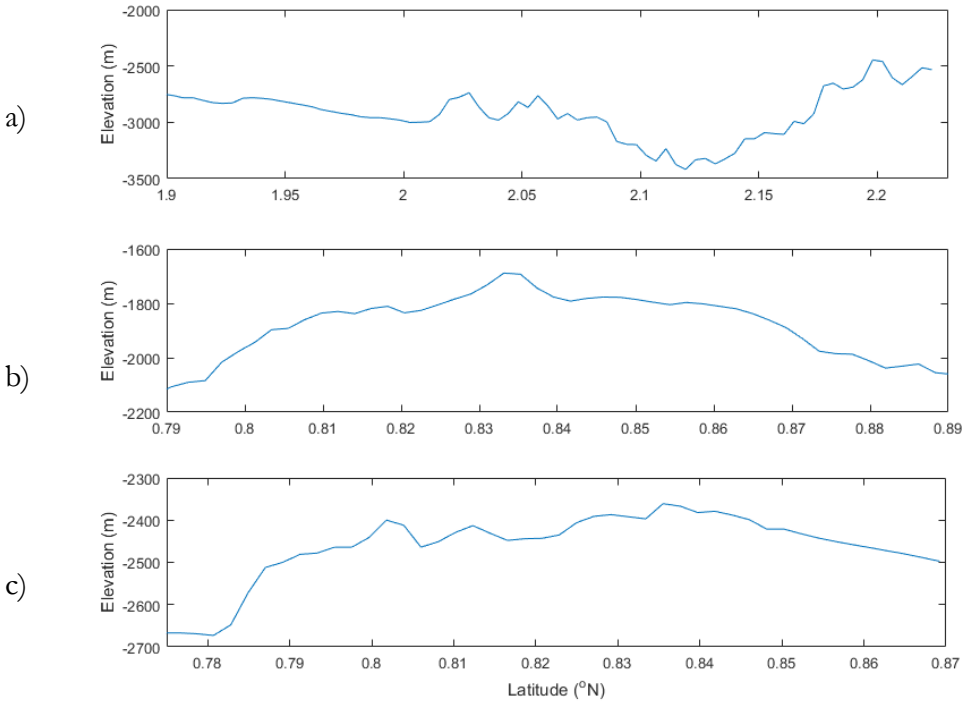

Figure 4: Axial ridge profiles along the GSC. Figure 4a displays the profile at an average longitude of 97.2°W. Figure 4b displays the profile view of the axial ridge at an average longitude of 89.6°W and Figure 4c displays the profile view of the axial ridge with an average longitude of 86.3°W

This information indicates the effect of hotspot swell on crustal thickness as the Galápagos hotspot is in close proximity to the GSC. The crustal thickness also changes due to the proximity to the hotspot. From 97°W to 91°25'W, it is apparent that the crustal thickness increases by 2.3 km (Canales *et al.*, 2002). Therefore, the crustal thickness changes along the GSC, which is important to note when considering depths of crystallization.

Cushman *et al.* (2004) determined that the crust is thickest (6.5-8 km thick) east of 92.6°W. It was also found that this crust was an "enriched" Mid Ocean Ridge Basalt (MORB) due to high K/Ti (>0.15) ratios. Between 92.6°W and 95.5°W crustal thickness ranges from 6-7 km (Cushman *et al.*, 2004). West of 95.5°W is the thinnest crust at less than 6 km and this area had K/Ti ratios between 0.09 and 0.15 signifying an area with Normal MORB. (Cushman *et al.*, 2004).

Previous work has been done to determine the depths within the crust that magmas reside. Colman *et al.* (2015) found that at 94.2°W, magma depths were around 2.6 km whereas at 95°W, the depths ranged from 3.0 to 3.4 km. Analysis of H_2O and CO_2 as well as seismic data was used to find these depths.

METHODS

Data were obtained from the recent compilation of glasses by Gale *et al.* (2014) and from online PetDB (Petrological Database). Other data compilations came from published papers by Cushman *et al.* (2004), Colman *et al.* (2012) and Colman *et al.* (2015) and will be incorporated further on in the methods. Sample locations for the Gale *et al.* (2014) glasses are shown in Figure 5. All 884 glasses were plotted in Figure 5 to establish the geographic distribution of analyses and to identify the spread of the data points and to make sure that the data used is on the ridge as opposed to samples collected away from the ridge axis (see Figure 3).

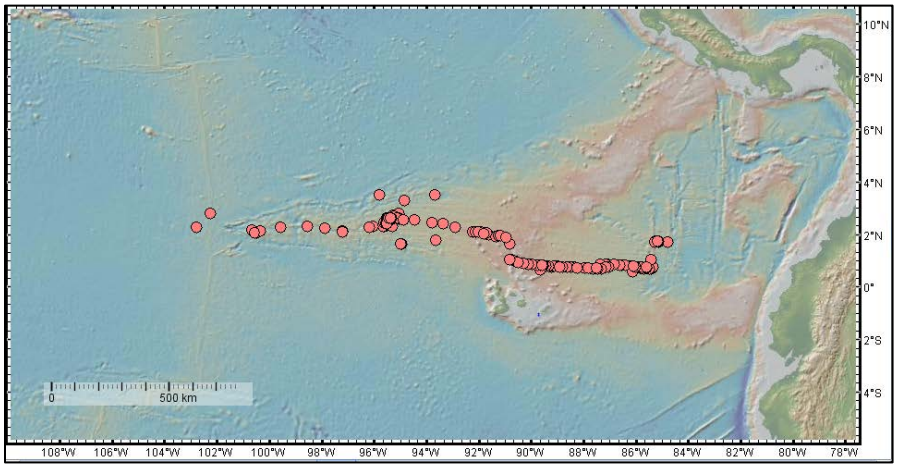

Figure 5: Locations of the original 884 samples before filtration. Only data on the GSC is useful to this research. Image created using *GeoMapApp*.

Only data on the GSC are useful for this research, therefore using Figure 5 to visually filter out the points that do not lie on the GSC was simple. Duplicate glasses could also be filtered out of the data, as overlap may have occurred from transferring the Gale *et al.* (2014) glass data and the PetDB data to one spreadsheet. After filtering the data, 790 analyses of lavas were compiled for the research project. The samples were divided into 12 sets, representing 12 different segments along the GSC. Each color signifies a different segment established using visual methods such as the amount of offset or separation from faulting (Figure 6). Segmentation will aid in understanding the GSC chemistry changes along the ridge and the pressure changes from segment to segment. This will help identify locations of interest and determine if the plumbing systems beneath the GSC is complex or simple. A simple plumbing system would be indicated by small variations in pressure and relatively shallow depths of crystallization.

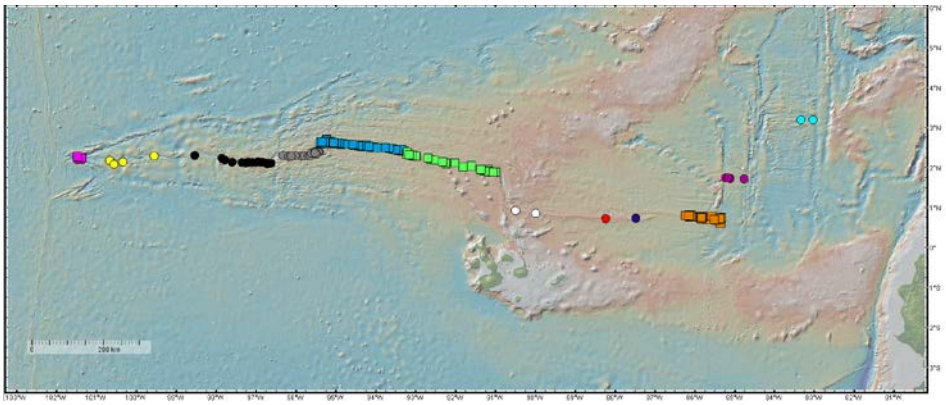

Figure 6: Shows the 12 segments after the filtration process. Image created using the *GeoMapApp*.

Using the relationships of the chemistry and pressure at each segment, segments can be evaluated and compared. Table 1 lists all the segments and how many data points are at each segment.

Table 1: Average longitudes and the number of samples for each segment for the Gale *et al.* (2014) dataset.

Segment	Color	Range of Longitudes		n
A	Pink	101.75°W	101.0°W	58
B	Yellow	101.75°W	98°9W	10
C	Black	98°9W	96.4°W	71
D	Grey	96.4°W	95.3°W	91
E	Blue	95.3°W	93.2°W	202
F	Green	93.2°W	90.8°W	96
G	White	90.8°W	89.0°W	3
H	Red	89.0°W	87.7°W	2
I	Navy	87.7°W	86.5°W	1
J	Orange	86.5°W	85.3°W	226
K	Purple	85.3°W	84.7°W	16
L	Cyan	84.7°W	82.9°W	14

The best way to view the changes of chemistry is to use Harker or variation diagrams. Harker diagrams use oxides to examine the relationships between different chemical elements, and to assess whether the observed relationships are consistent with the compositional changes expected from crystallization. Oxides are plotted against MgO in weight percent, where MgO is used as an index of differentiation because MgO shows a relatively wide range of crystallization in basalts reflecting

crystallization of olivine, and also provides an indication of the variation in temperatures of basaltic magmas (Langmuir *et al.* 1992).

Pressures of partial crystallization were calculated using the method described by Kelley and Barton (2008). The Gale *et al.* (2014) data had already been normalized to 8 wt.% MgO. The average of three pressure calculations is used to calculate pressures for melts in equilibrium with olivine, plagioclase and clinopyroxene. Results are considered valid if the uncertainty in the calculated pressure is less than 126 MPa (Kelley and Barton 2008). Some calculated pressures have negative values. Those associated with uncertainties greater than 126 MPa are clearly erroneous and are discarded from the results, whereas negative pressures between 0.1 and -126 MPa are equal to atmospheric pressure within uncertainty and are assumed to be .01 MPa (Kelley and Barton 2008).

Glass data from Cushman *et al.* (2004), Colman *et al.* (2012) and Colman *et al.* (2015) were also used to calculate pressures using the Kelley and Barton (2008) method. Analyses of 134 glass samples were obtained from Cushman *et al* (2004). Locations are given for 112 of the 134 glasses, and these 112 analyses were used for this research. Colman *et al.* (2012) reported glass analyses for 331 samples, and Colman *et al.* (2015) reported analyses for another 79 and all of these samples were added to the data set. Figure 7 shows the distribution of these new data along the GSC. The data of Cushman *et al* (2004) and Colman *et al.* (2012, 2015) were assigned to the segments defined using the Gale *et al.* (2014) data. Comparison between results obtained with these data, and those obtained with the Gale *et al.* (2014) is left to the discussion.

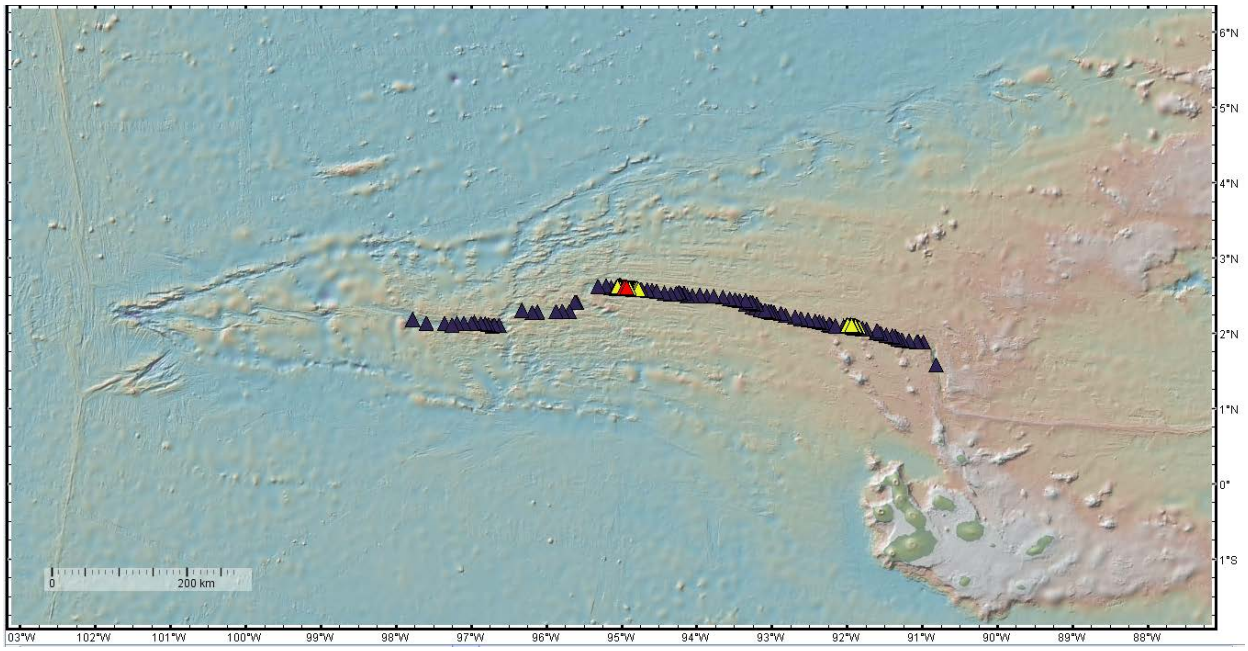

Figure 7: Distribution of the new data. Cushman *et al.* (2004) is the dark blue, Colman *et al.* (2012) is yellow and Colman *et al.* (2015) is red.

RESULTS

A plot of the average pressure calculated for samples from each segment versus the average value of longitude for the segment is shown in Figure 8. The values for highest and lowest pressures are also shown for each segment. The average pressures of partial crystallization are relatively constant along the ridge, and for most segments, the calculated average pressures are consistent with partial crystallization within the crust at average depths from 1.6 km to 10.7 km. However, anomalously high pressures were calculated for some segments (e.g. those near the transform fault at 86°W and to the west of the Galápagos Islands) and indicate unrealistically high nominal depths of crystallization with values up to 26 km.

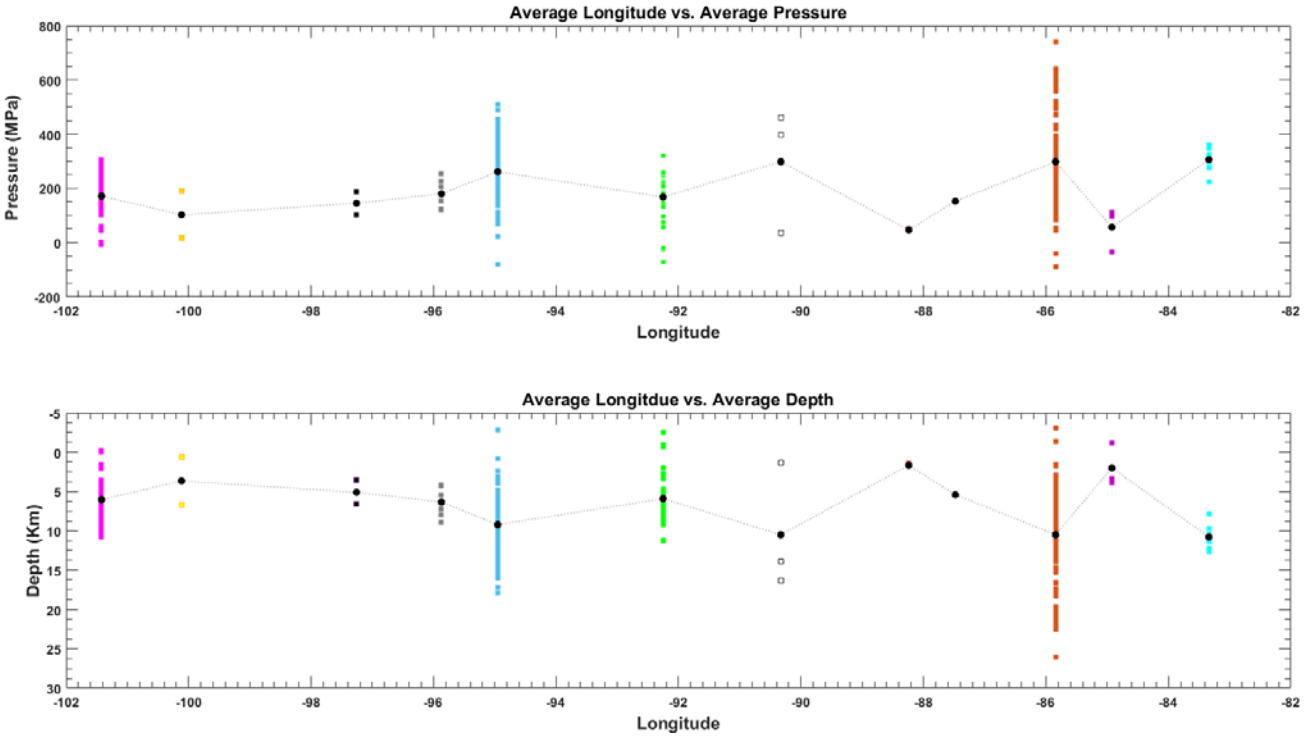

Figure 8: Describes the range of pressures and depths as well as the average pressures and depths along the Galápagos Spreading Center. The average longitude at each segment is connect to easily show the range of calculated averages.The longitude is an average longitude taken from each segment. Summary of the data can be seen in Table 1. Colors match that of Figure 2.

Four segments (A, E, F and J) were examined in greater detail to obtain information about changes in magma chemistry and in the pressures of partial crystallization along the GSC. Segment A, the westernmost segment on the GSC with an average longitude of 101.4°W, was the first of four segments to be evaluated further. This segment is of interest due to the proximity of the segment to the triple junction and as it is a propagating tip. The average spreading rate at this segment is 40.39 mm/year (Gale et al. 2014) and the average pressure of partial crystallization is 171.4 Mpa, corresponding to a depth of 6 km. Calculated pressures are all below 307 MPa (Figure 9). The inverse correlation of CaO vs MgO and CaOAl2O3 vs MgO are consistent with the crystallization of pyroxene along with olivine and plagioclase. The enrichment of K_2O as crystallization proceeds is

greater than that of P_2O_5. These oxides both show highly incompatible behavior during crystallization, so that the data suggest the processes other than crystallization (such as crustal assimilation) have occurred at this segment.

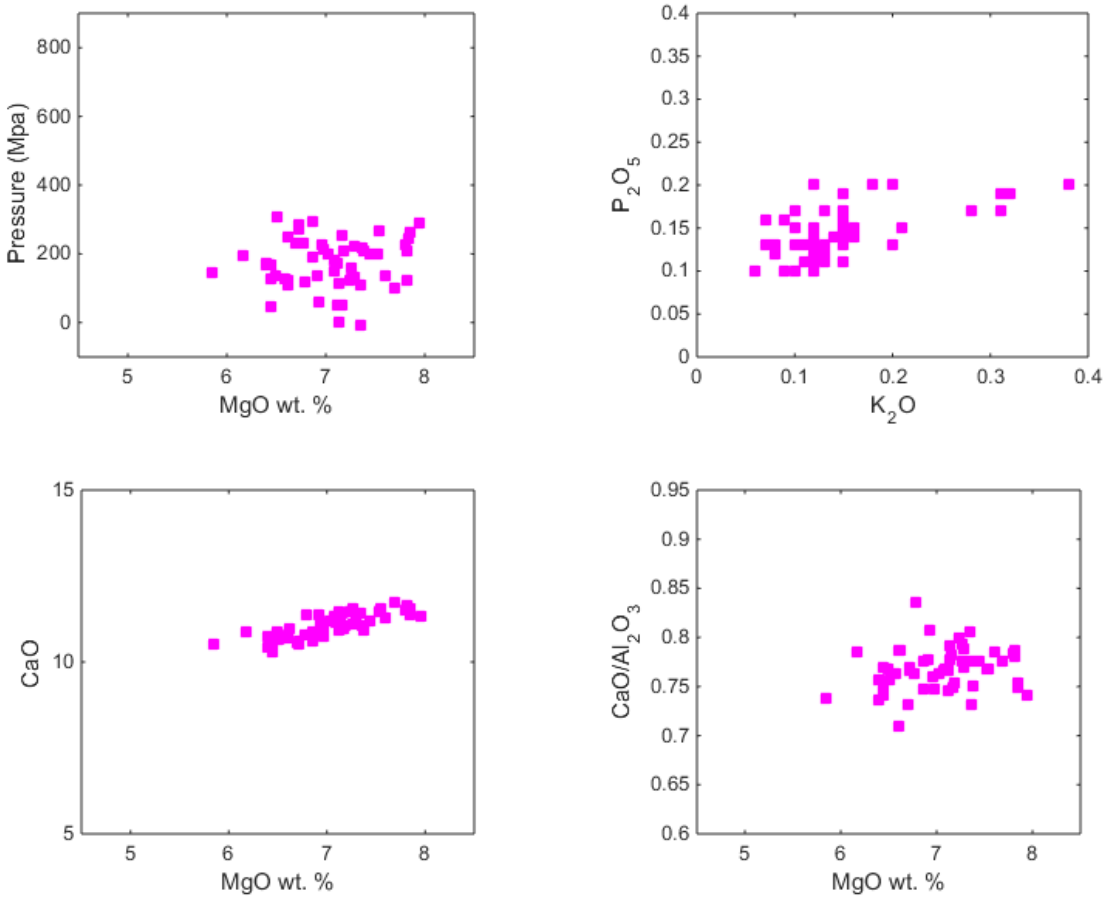

Figure 9: Four chemistry plots created for segment A using the Gale *et al.* (2014) data. Average longitude is 101.42°W.

Segment E has an average longitude of 94.9°W and an average spreading rate of 50.57 mm/year (Gale *et al.* 2014). The average calculated pressure is 261.6 MPa. Pressures are approximately constant as a function of MgO, and indicated crystallization at an average depth of 9.21 km. Figure 10 displays an interesting trend of pressures. The negative trends of CaO vs MgO and $CaOAl_2O_3$ vs MgO are consistent with the crystallization of pyroxene along with olivine and plagioclase. As at segment A, the enrichment of K_2O as crystallization proceeds is greater than that of P_2O_5. These oxides both show highly incompatible behavior during crystallization, so that the data suggest the processes other than crystallization, such as crustal assimilation, have also occurred at this segment.

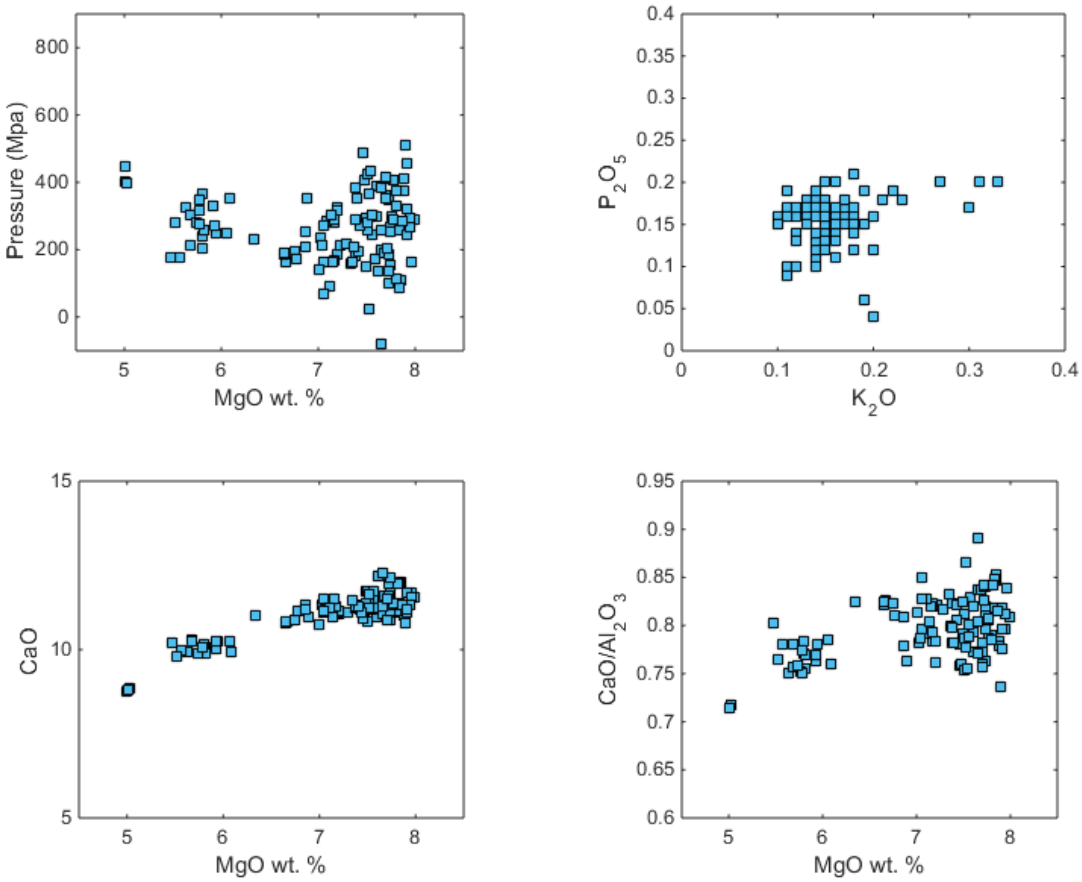

Figure 10: Harker diagrams for segment E using the Gale *et al.* (2014) data set.

Segment F has an average longitude of 92.2°W and a spreading rate between 53.05 mm/year and 54.93 mm/year (Gale *et al.* 2014). The segment is the closest to the Galápagos Archipelago, and therefore the closest to the Galápagos hotspot The average pressure at this segment is 168.2 MPa, lower than at segment E. This pressure corresponds to an average depth of crystallization of 5.91 km. Figure 11 shows that the chemistry of samples from segment F is consistent with crystallization of olivine, plagioclase and clinopyroxene. However, as at segments A and E, the enrichment of K_2O as crystallization proceeds is greater than that of P_2O_5, suggesting that processes other than crystallization (such as crustal assimilation) have also occurred at this segment.

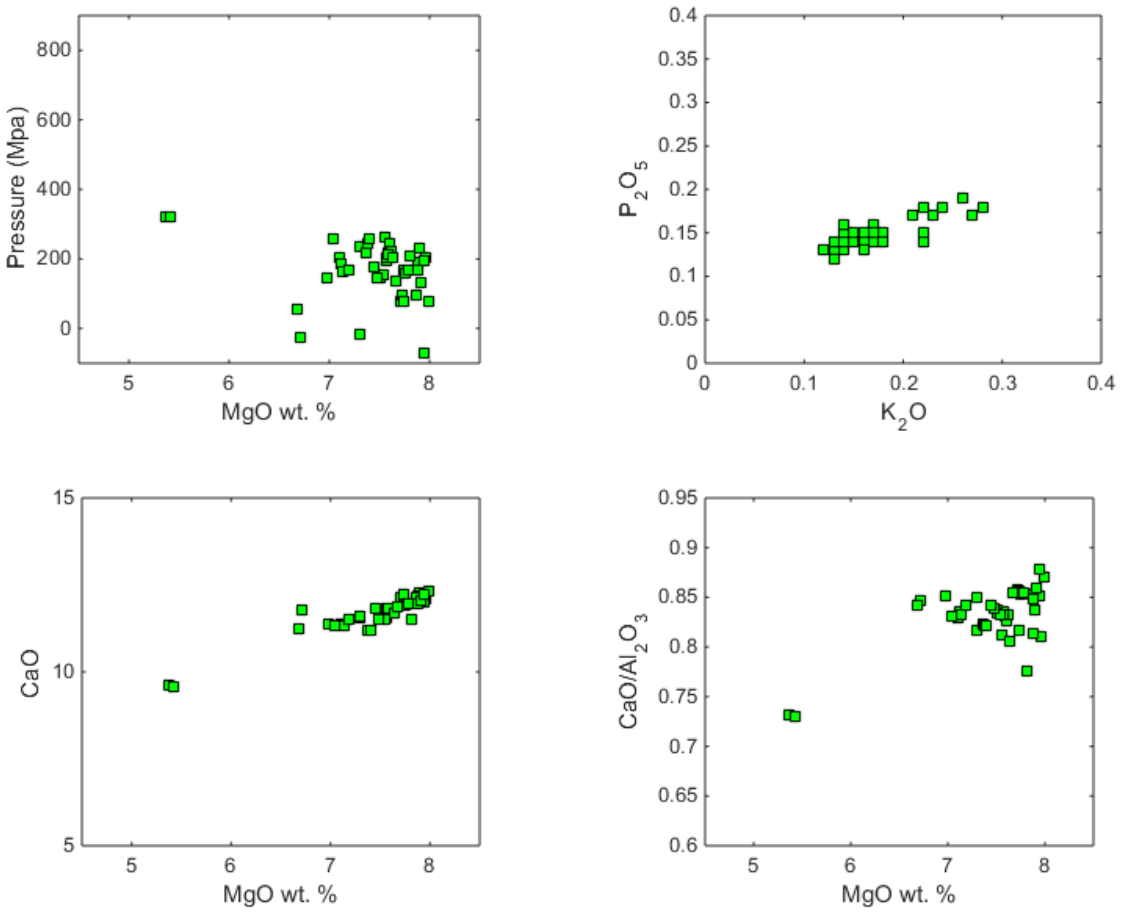

Figure 11: Harker diagrams for segment F using the Gale et al. (2014) data.

Segment J, at an average longitude of 85.8°W, has an average spreading rate of 62.62 mm/year (Gale et al. 2014). The average calculated pressure is 298.3 Mpa, corresponding to an average depth of 10.49 km. Figure 12 displays the Harker diagrams for this segment. The observed variations are consistent with crystallization of olivine, plagioclase and clinopyroxene. However, in contrast to the results for segments A, E, and F, the enrichment of K_2O as crystallization proceeds is about the same as that for P_2O_5, suggesting that crystallization was the dominant process along this segment. Another unusual feature is the tendency for evolved lavas (lower MgO) to yield higher pressures than the least evolved magmas. The negative correlation between pressure and MgO is difficult to explain by crystallization alone. Segment J is adjacent to a large transform fault, and understanding how this transform fault effects the chemistry of the magmas erupted along the ridge is important for understanding the dynamics of sea-floor spreading.

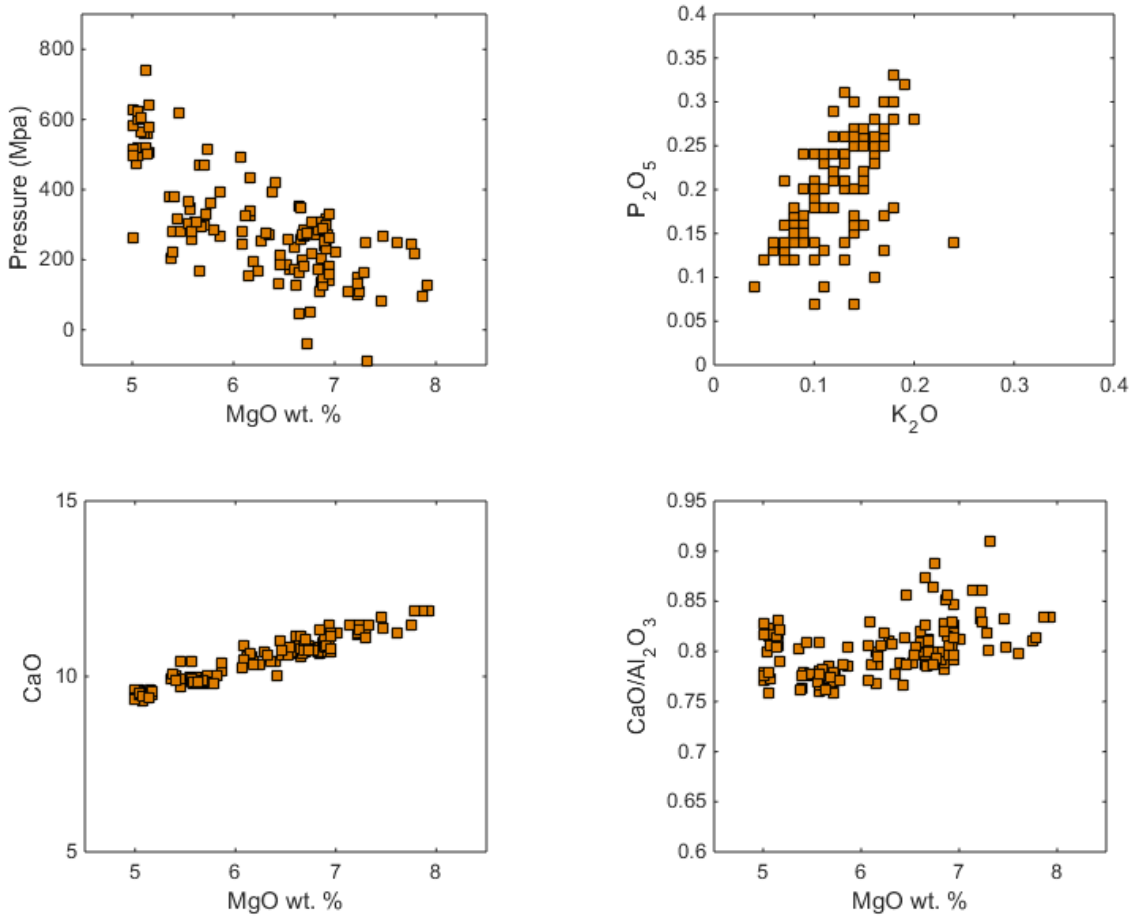

Figure 12: Variation diagrams for segment J, near the transform fault.

Figure 13 shows a plot of all glasses from segments A, E, F and J. Samples from segment A (near the triple junction) are anomalously rich in Na_2O and have high values of Na_8 (Na_2O concentration calculated at 8 wt% MgO) whereas samples from segment J (near the transform) have low values of Na_8.This diagrams serves to emphasize the fact that samples from segments A, E and F show relationships of P_2O_5 with K_2O that are inconsistent with magma evolution via crystallization. This suggests the possibility that some magmas interacted with pre-existing oceanic crust *en-route* to the surface.

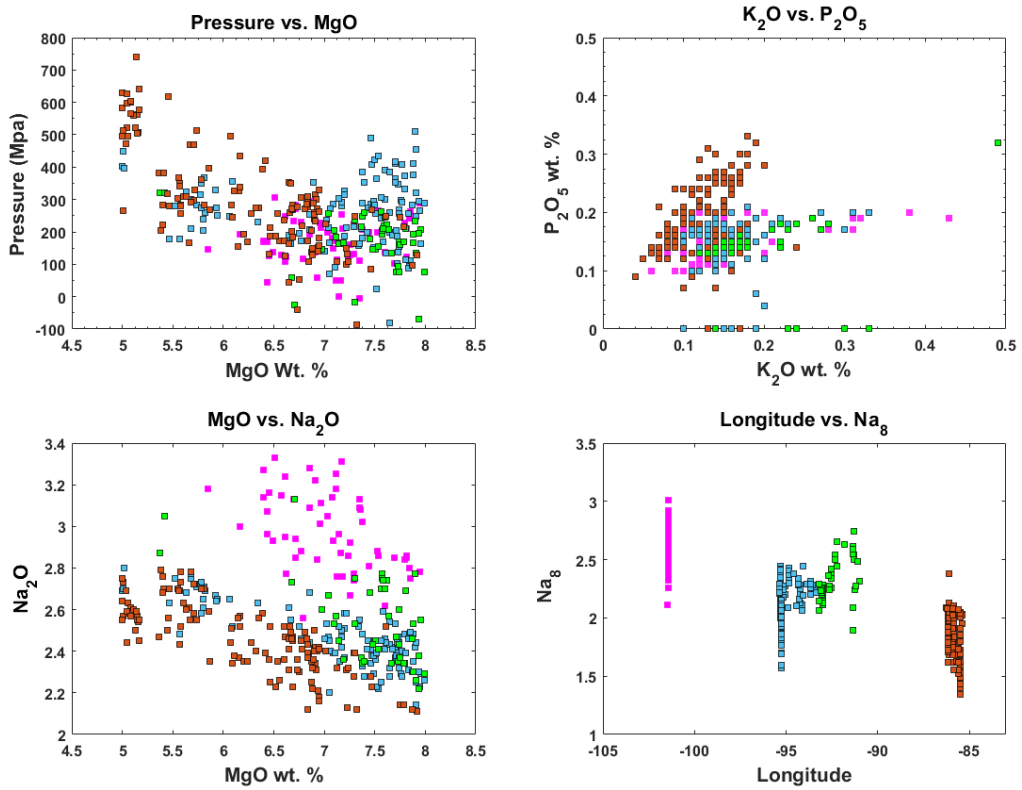

Figure 13: Relationships between four of the twelve segments along the Galápagos Spreading Center. Colors can be matched from Figure 2. The pink is segment A, starting from the west of the GSC. A summary of these data is given in Table 1.

The next step is comparison of the glass data from Cushman *et al.* (2004), Colman *et al.* (2012) and Colman *et al.* (2015) to the Gale *et al.* (2014) glasses. Overall, the data show similar results with the Gale *et al.* (2014) data. This is encouraging because it suggests consistency in the methods used to analyze the data as well as consistency in the data themselves. More data is necessary to better establish chemical variations along the Galápagos Spreading Center, but it can now be assumed that the Gale *et al.* (2014) data provide a reasonably accurate picture of the pressures of partial crystallization and of the variations in lave composition along this ridge.

Figure 14 displays the comparison of the new data to the Gale *et al* (2014) data for Segment E. Overall, the data sets and the results obtained for the pressures of partial crystallization are consistent with each other. High pressure values are associated with higher MgO and lower Na_2O and occur mostly at the western end of the segment at around 95.4°W. The array of points on the plot of P_2O_5 vs. K_2O indicates enrichment of these elements at about the same rate, in contrast to the Gale *et al.* (2014) data, implying that the concentrations of these oxides is largely controlled by crystallization.

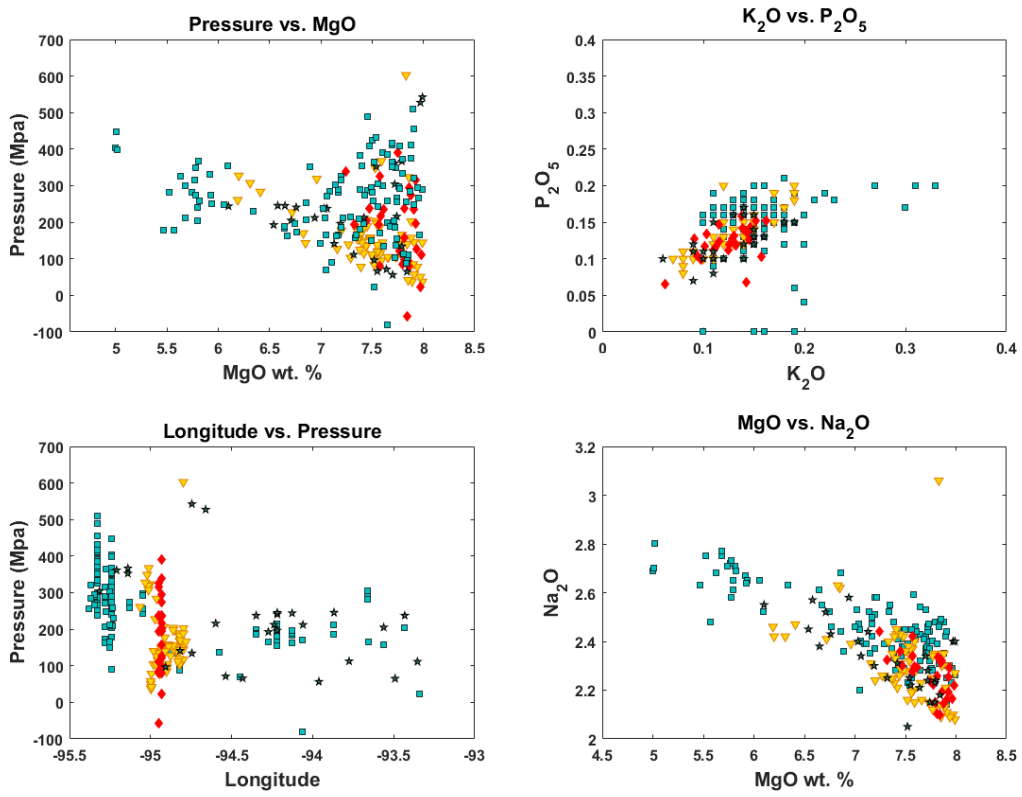

Figure 14: Comparison of Gale *et al.* (2014) with added data for segment E.. The yellow triangle is the Colman *et al.* (2012) data, the red diamond is the Colman *et al.* (2015) data, the star is the Cushman *et al.* (2004) data and the blue box is the Gale *et al.* (2014) data.

Figure 15 displays the comparison of the new calculations from Colman *et al.* (2012) and Cushman *et al.* (2004) to the Gale *et al.* (2014) data for segment F. The Colman *et al.* (2015) glasses did not have any data points in this region of the GSC. Again, the data sets and the results obtained for the pressures of partial crystallization are consistent with each other. The Colman *et al.* (2012) data extend the compositional range of lavas from this segment to lower MgO values., and establish relatively low pressures of partial crystallization over a wide range of MgO contents. However, both the Colman *et al.* (2012) and Cushman *et al.* (2004) samples yield some higher pressures than the Gale *et al.* (2014) data for samples with higher MgO contents.

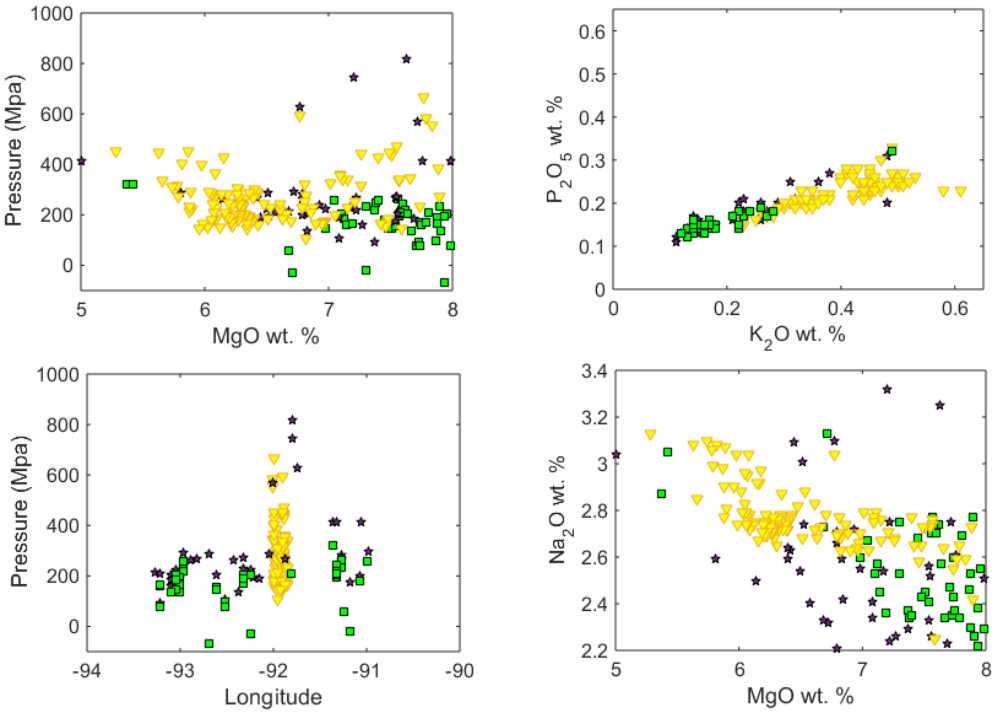

Figure 15: The new data from Colman *et al.* (2012) and Cushman *et al.* (2004) to the Gale *et al.* (2014) data at segment F. The yellow triangle is the Colman *et al.* 2012 data, the star is the Cushman *et al.* (2004) data and the green box is the Gale *et al.* (2014) data.

DISCUSSION

With the Kelley and Barton (2008) method, some of the calculated pressures need to be filtered out of the results. Their method is only appropriate for melt compositions (glasses) in equilibrium with (crystallizing) olivine, pyroxene, and plagioclase. Examination of major-oxide analyses of mid-ocean ridge basalts indicates that only melts (glasses) containing between 5 and 8 wt.% MgO are in equilibrium with these phases (Langmuir *et al.* 1992). Therefore, all samples with MgO greater than 8 wt.% and less than 5 wt.% were filtered out of the results. Figure 16 shows all 790 glasses together, and shows those glasses that yield valid estimates of the pressures of partial crystallization.

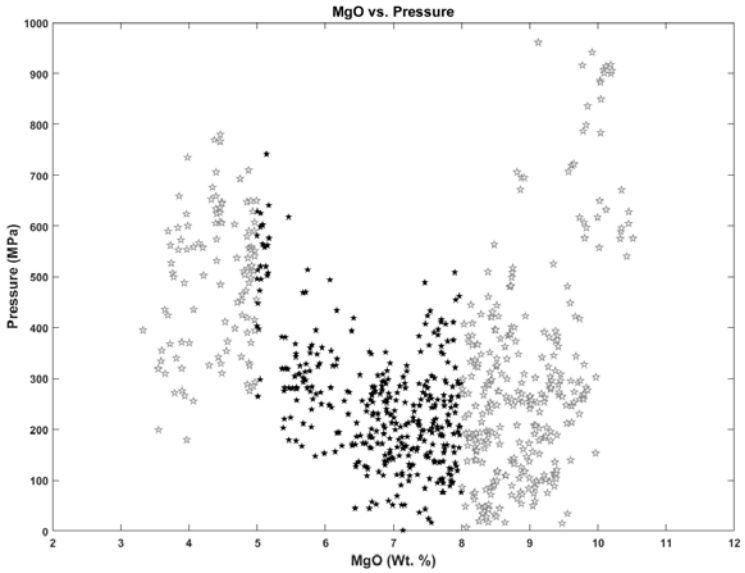

Figure 16: The calculated pressures of the 790 data points plotted against MgO. The dark grey points represent calculated pressures that are considered to represent reliable results.

After filtering, the number of samples yielding reliable calculated pressures is 368. Results for these samples were plotted by their corresponding segments in order to examine the change in distribution (from Figure 6 to Figure 16) and to determine what segments could best identify the changes of chemistry along the GSC. Figure 17 displays the distribution of the 368 glasses.

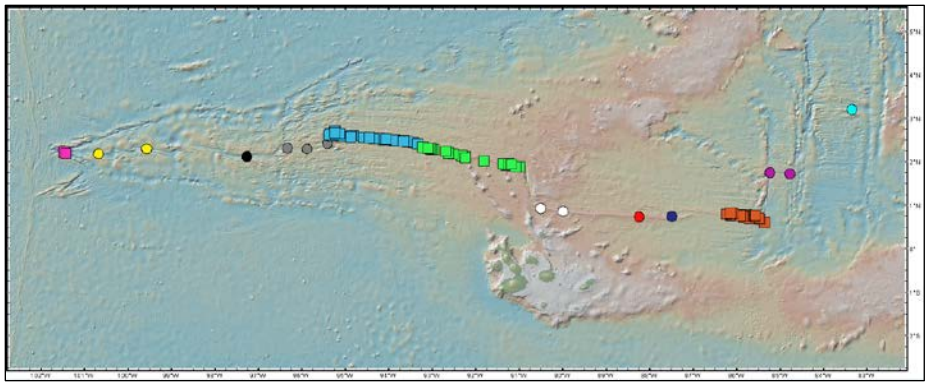

Figure 17: Twelve segments after the MgO values above 8 wt. % and below 5 wt. % were filtered out. Image created using the GeoMapApp.

Table 2 shows the range of pressures for the full data set and the range of pressures for the filtered data set as well as the number of samples before and after filtration. The number of samples per segment is important when determining those segments that will provide the most reliable trend of pressure versus longitude. For this reason, in the results section, segments A, E, F and J were chosen for more detailed discussion.

Table 2: Original pressure ranges and number of glasses as well as the number of glasses and the range of pressures after pressure filtration.

		Original Pressure			Pressures after filtration		
Segment	Color	n_1	Range of P (MPa)	Average P (MPa)	n_2	Range of P (MPa)	Avg P (MPa)
A	Pink	58	.01-406.7	181.2	54	.01-307.2	171.4
B	Yellow	10	16.2-941.7	500.8	2	16.2-189.1	102.7
C	Black	71	.01-917.3	338.42	2	102.9-187.4	145.1
D	Grey	91	.01-835.6	282.3	6	118.8-253.4	180.2
E	Blue	202	.01-517.76	251.8	114	.01-508.7	261.6
F	Green	96	.01-695.4	225	45	.01-319.7	168.2
G	White	3	36.4-462.1	298.3	3	36.4-462.1	298.3
H	Red	2	42.8-50.8	46.85	2	42.8-50.8	46.85
I	Navy	1	152.5	152.5	1	152.5	152.5
J	Orange	226	.01-779.6	389.9	129	.01-741.384	298.3
K	Purple	16	.01-426.2	200.7	3	.01-110.551	56.8
L	Cyan	14	48.3-360.9	258.1	7	223.3-360.9	306

Pressure filtration is also necessary for the Cushman *et al.* (2004), Colman *et al.* (2012) and Colman *et al* (2015) glasses. Table 3 displays the new data after pressure filtration. It is apparent that only segments E and F can be compared to the Gale *et al.* (2014) glasses due to the amount of samples in each segment.

Table 3: Shows average data for added data sets from Cushman 2004, Colman 2012 and Colman 2015.

	Segment	Avg. Pressure (Mpa)	Avg. Long	St. Dev. (Mpa)	Min Pressure (Mpa)	Max Pressure (Mpa)	# of Samples	Z Avg (km)
	Cushman *et al.* (2004)							
A	C	106.71	-97.08	53.06	38.74	186.63	4	3.77
	D	188.11	-96.13	73.43	125.38	297.16	3	6.6
	E	222.02	-94.34	124.42	56.24	542.54	27	7.81
	F	284.36	-92.25	158.83	93.94	818.88	38	10
	Colman *et al.* (2012)							
B	E	164.45	-94.9	92.9	37.33	602.46	63	5.7866
	F	265.5	-91.93	103.23	104.52	668.3	120	9.34
	Colman *et al.* (2015)							
C	E	185.24	-94.93	103.74	0.01	389.66	26	6.5

CONCLUSIONS

This work has shown that both the chemical compositions of erupted lavas and calculated pressures of partial crystallization vary along the GSC. This implies that the processes operating beneath this ridge may be a more complex model of crustal accretion.

The largest range of pressures is observed for samples from segment J, near a large transform fault. For the samples from this segment, there is an unusual (and improbable) negative correlation between P and MgO, and values of Na_8 are the lowest of all samples erupted along the GSC, implying higher degrees of melting at what should be a cooler part of the GSC. These unusual characteristics suggest that processes other than crystallization have occurred in the crust beneath this ridge segment.

Samples from segment A, near the ridge-ridge intersection (triple junction), have high Na_2O and Na_8 compared to samples erupted along other segments. This suggests that these magmas were produced by lower degrees of melting in the mantle source region. This seems to be consistent for magmas formed at a propagating ridge tip. The low Na_2O does not seem to have any dramatic effect on calculated pressures (Figure 3).

During crystallization, P_2O_5 and K_2O should vary with a ~1:1 ratio. The P_2O_5 and K_2O contents of many samples from the GSC deviate from this ratio, suggesting that crystallization of these magmas was accompanied by interaction with pre-existing crust. The high (relative to K_2O) P_2O_5 content of samples from segment J probably accounts for the wide range of pressures calculated for samples from this segment. However, this idea needs to be tested in future work.

The data from Cushman *et al.* (2004), Colman *et al.* (2012), and Colman *et al.* (2015) have compositions that are broadly consistent with those reported by Gale *et al.* (2014), and can be used with the latter to examine chemical variations along the GSC. Additional data are still necessary to better establish the geochemical variations for segments for which there are still only relatively few samples. Additional data will also help establish more consistent geochemical trends, for segments with a relatively large number of existing sample, such as segment E and F.

Though a model of crustal accretion could not be determined in this work, the results suggest crystallization over a range of pressure, and hence depth, and that the gabbro-glacial model is not appropriate for this ridge. However, refinement of the results obtained in this work, together with results obtained from new samples, is needed to identify the correct model for crustal accretion and to place constraints on crustal thickness.

RECOMMENDATIONS FOR FUTURE WORK

Research continues on magmatism along the Galápagos spreading center. Efforts are underway to find evidence for intra-crustal processes such as mixing and assimilation, and to determine whether the operation of such processes accounts for the anomalously high pressures of partial crystallization calculated for some ridge segments. Future work should also include efforts to interpret calculated pressures in terms of crustal thickness and to compare pressures of partial crystallization calculated for the GSC with those calculated for other ridges such as the East Pacific Rise. This research will also serve as a basis for determining a model of crustal accretion at the GSC in future work. Acquisition of additional rock samples for petrographic analysis will be used in order to observe the processes that are occurring along the GSC.

REFERENCES CITED

Bedard, J H, Lauziere, K, Tremblay, A, Sangster, A, 1998, Evidence for forearc seafloor-spreading from the Betts Cove ophiolite, Newfoundland: oceanic crust of boninitic affinity: Tectonophysics, v. 284, p. 233-245.

Boudier, F., Nicolas, A., Ildefonse, B., 1996, Magma chambers in the Oman ophiolite: fed from the top and the bottom: Earth and Planetary Science Letters, v. 144, p. 239-250.

Bryan, W. B., Moore, J. G., 1977, Compositional variations of young basalts in the Mid-Atlantic Ridge rift valley near lat 36°49'N: Geological Society of America Bulletin, v. 88, p. 556-570.

Canales, J.P., Ito, G., Detrick, R. S., Sinton, J., 2002, Crustal thickness along the western Galápagos Spreading Center and the compensation of the Galapagos hotspot swell: Earth and Planetary Science Letters, v. 203, p. 311-327.

Colman, A., Sinton, J M., Wanless,V. D., 2015, Constraints from melt inclusions on depths of magma residence at intermediate magma supply along the Galápagos Spreading Center: EPSL Earth and Planetary Science Letters, v. 412, p. 122-131.

Colman, A., Sinton, J M., White, S M., McClinton, J. T., Bowles, J. A., Rubin, K. H., Behn, M. D., Cushman, B., Eason, D. E., Gregg, T. K. P., Grönvold, K., Hidalgo, S., Howell, J., Neill, O., Russo, C., 2012, Effects of variable magma supply on mid-ocean ridge eruptions: Constraints from mapped lava flow fields along the Galápagos Spreading Center: Geochemistry, Geophysics, Geosystems, v. 13, n. 8. doi:10.1029/2012GC004163

Cushman, B., Sinton, J., Ito, G., Eaby Dixon, J., 2004, Glass compositions, plume-ridge interaction, and hydrous melting along the Galápagos Spreading Center, 90.5°W to 98W: Geochemistry, Geophysics, Geosystems, v. 5, n. 8. doi:10.1029/2004GC000709

Dewey, J. F., Kidd, W.S.F., 1977, Geometry of plate accretion: Geol Soc America Bull Geological Society of America Bulletin, v. 88, p. 960-968.

Gale, A., Langmuir, C H., Dalton, C A., 2014, The Global Systematics of Ocean Ridge Basalts and their Origin. Journal of Petrology, v. 55, p. 1051-1082.

Harpp, K., Geist, D. 2002, Wolf-Darwin lineament and plume-ridge interaction in northern Galápagos: Geochemistry, Geophysics, Geosystems, v. 3, n. 11. Doi: 10.1029/2001GC000225

Hey, R., 1977, Tectonic evolution of the Cocos-Nazca spreading center: Geol Soc America Bull Geological Society of America Bulletin, v. 88, p. 1404-1420.

Kelemen, P B, Koga, K, Shimizu, N, 1997, Geochemistry of gabbro sills in the crust-mantle transition zone of the Oman ophiolite: Implications for the origin of the oceanic lower crust: Earth and Planetary Science Letters., v. 146, p. 475-488.

Kelemen, P. B., Aharanov, E., 1998, Periodic Formation of Magma Fractures and Generation of Layered Gabbros in the Lower Crust Beneath Oceanic Spreading Ridges: Geophysical Monograph., v. 106, p. 267-289.

Kelley, D. F., Barton, M., 2008, Pressures of Crystallization of Icelandic Magmas: Journal of Petrology, v. 49, p. 465-492.

Langmuir, C. H., E. M. Klein, and T. Plank., 1992, Petrological Systematics of Mid-ocean Ridge Basalts: Constraints on Melt Generation beneath Ocean Ridges. Mantle Flow and Melt Generation at Mid-Ocean Ridges Geophysical Monograph Series v. 71, p.183-280.

Quick, J. E., Denlinger, R. P., 1993, Ductile deformation and the origin of layered gabbro in ophiolites: JGRB Journal of Geophysical Research: Solid Earth, v. 98, p. 14015-14027.

Rubin K.H., Sinton J.M., Hellebrand E., MacLennan J., 2009, Magmatic filtering of mantle compositions at mid-ocean-ridge volcanoes: Nat. Geosci. Nature Geoscience, v. 2, p. 321-328.

Sinton, J. M., Detrick, R. S., 1992, Mid-ocean ridge magma chambers: Journal of Geophysical Research: Solid Earth, v. 97, p. 197-216.

Sleep, N.H., 1975, Formation of oceanic crust: Some thermal constraints: Journal of Geophysical Research, v. 80, p. 4037-4042.

APPENDIX

Due to the amount of data used in this research, a separate file will be uploaded to the Knowledge Bank with supplementary materials.